MicroRNA396-Targeted *SHORT VEGETATIVE PHASE* Is Required to Repress Flowering and Is Related to the Development of Abnormal Flower Symptoms by the Phyllody Symptoms1 Effector[1]

Chiao-Yin Yang[2], Yu-Hsin Huang[2], Chan-Pin Lin[2], Yen-Yu Lin, Hao-Chun Hsu, Chun-Neng Wang, Li-Yu Daisy Liu, Bing-Nan Shen, and Shih-Shun Lin*

Institute of Biotechnology (C.-Y.Y., Y.-H.H., C.-P.L., Y.-Y.L., B.-N.S., S.-S.L.), Genome and Systems Biology Degree Program (S.-S.L.), Department of Plant Pathology and Microbiology (C.-Y.Y., Y.-H.H., C.-P.L., Y.-Y.L.), Institute of Ecology and Evolutionary Biology, Department of Life Science (H.-C.H., C.-N.W.), and Department of Agronomy (L.-Y.D.L.), National Taiwan University, Taipei 106, Taiwan; and Agricultural Biotechnology Research Center, Academia Sinica, Taipei 115, Taiwan (S.-S.L.).

ORCID IDs: 0000-0002-9951-687X (C.-P.L.); 0000-0002-7295-5004 (S.-S.L.).

Leafy flowers are the major symptoms of peanut witches' broom (PnWB) phytoplasma infection in *Catharanthus roseus*. The orthologs of the phyllody symptoms1 (PHYL1) effector of PnWB from other species of phytoplasma can trigger the proteasomal degradation of several MADS box transcription factors, resulting in leafy flower formation. In contrast, the flowering negative regulator gene *SHORT VEGETATIVE PHASE* (*SVP*) was up-regulated in PnWB-infected *C. roseus* plants, but most microRNA (miRNA) genes had repressed expression. Coincidentally, transgenic Arabidopsis (*Arabidopsis thaliana*) plants expressing the *PHYL1* gene of PnWB (*PHYL1* plants), which show leafy flower phenotypes, up-regulate *SVP* of Arabidopsis (*AtSVP*) but repress a putative regulatory miRNA of *AtSVP*, miR396. However, the mechanism by which PHYL1 regulates *AtSVP* and miR396 is unknown, and the evidence of miR396-mediated *AtSVP* degradation is lacking. Here, we show that miR396 triggers *AtSVP* messenger RNA (mRNA) decay using genetic approaches, a reporter assay, and high-throughput degradome profiles. Genetic evidence indicates that *PHYL1* plants and *atmir396a-1* mutants have higher *AtSVP* accumulation, whereas the transgenic plants overexpressing *MIR396* display lower *AtSVP* expression. The reporter assay indicated that target-site mutation results in decreasing the miR396-mediated repression efficiency. Moreover, degradome profiles revealed that miR396 triggers *AtSVP* mRNA decay rather than miRNA-mediated cleavage, implying that *AtSVP* caused miR396-mediated translation inhibition. We hypothesize that PHYL1 directly or indirectly interferes with miR396-mediated *AtSVP* mRNA decay and synergizes with other effects (e.g. MADS box transcription factor degradation), resulting in abnormal flower formation. We anticipate our findings to be a starting point for studying the posttranscriptional regulation of PHYL1 effectors in symptom development.

Phytoplasmas are obligate bacteria without cell walls that infect numerous plants, causing severe agricultural losses (Lee et al., 2000). The typical symptoms on phytoplasma-infected plants include witches' broom, proliferative branches, leaf yellowing, and small leaves (Lee et al., 2000). The flowers of infected plants exhibit sterility, abnormal morphology, virescence, and phyllody (herein referred to as leafy flower; Himeno et al., 2011). Peanut witches' broom (PnWB) phytoplasma-infected *Catharanthus roseus* plants exhibit leafy flower symptoms, which were classified into five stages depending on their severity as described previously (Yang, 1985; Liu et al., 2014). Stage 4 (S4) leafy flowers exhibited leaf vein patterning with phyllody petals and intumescent ovaries (Fig. 1A; Liu et al., 2014).

The draft genome sequence of the PnWB phytoplasma contains 13 chromosomal contigs with 562,473 bp and 421 protein-coding genes (Chung et al., 2013). Chung et al. (2013) suggested that the 48 putative PnWB effectors are similar to known pathogenicity effectors of phytoplasmas. In aster yellows witches' broom (AYWB)
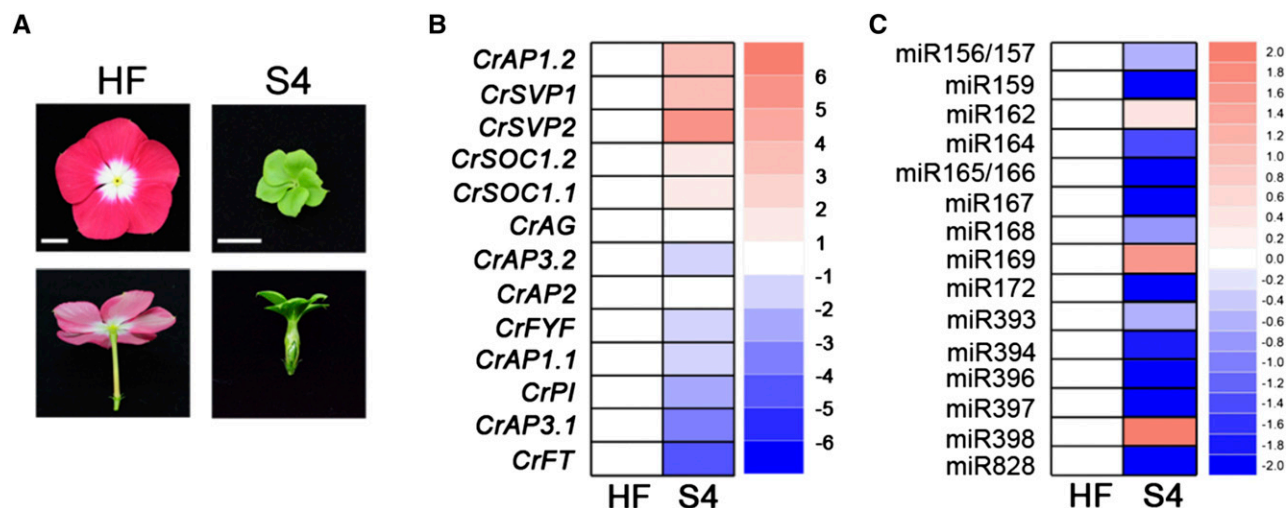
Figure 1. The leafy flower phenotypes of PnWB phytoplasma-infected *C. roseus* plants. A, The healthy flower (HF) and S4 PnWB-infected leafy flower symptoms are presented in the left and right columns, respectively. Bars = 1 cm. B and C, The mRNA (B) and microRNA (miRNA; C) expression of the HF and S4 in *C. roseus* flowers are represented by heat maps. Red indicates up-regulated expression, and blue indicates down-regulated expression. The values at right indicate the results of the $\log_2$ (S4/HF) formula. *CrAG, AGAMOUS* of *C. roseus; CrFYF, FOREVER YOUNG FLOWER* of *C. roseus; CrPI, PISTILLATA* of *C. roseus*.

phytoplasma, the secreted AYWB PHYTOPLASMA PROTEIN54 effector (SAP54) causes a leafy flower phenotype in transgenic Arabidopsis (*Arabidopsis thaliana*) plants (*SAP54* plants; MacLean et al., 2011). Moreover, the phyllody symptoms1 (PHYL1) effector of onion yellows phytoplasma wild-type line, a SAP54 ortholog, also manifested an identical leafy flower phenotype in *PHYL1*-overexpressing plants (Maejima et al., 2014).

PHYL1 and SAP54 interact with MADS domain transcription factors (MTFs) in Arabidopsis, such as SEPALLATA3 (AtSEP3), APETALA1 (AtAP1), and CAULIFLOWER (AtCAL; MacLean et al., 2014; Maejima et al., 2014). These MTFs are key regulators in floral development and were triggered by SAP54/PHYL1-mediated ubiquitin/26S proteasomal degradation by interacting with the RADIATION SENSITIVE23 (RAD23) family, resulting in interference in floral homeotic gene expression levels (MacLean et al., 2014; Maejima et al., 2014). Consistently, the *ap1* mutant, *ap1/cal* double mutant, and *sep1/sep2/sep3/sep4* quadruple mutant manifest various types of leafy flower (e.g. leaf-like sepals, secondary flowers, cauliflower-like inflorescences, or loss of floral meristem determinacy; Bowman et al., 1993; Ditta et al., 2004; Gregis et al., 2006). These results suggest that phytoplasma SAP54/PHYL1 is a key effector for triggering positive regulators of MTF degradation to switch the phase transition of plants from the reproductive stage to the vegetative stage.

In PnWB-infected *C. roseus* plants, the expression levels of *SHORT VEGETATIVE PHASE1* (*CrSVP1*) and *CrSVP2* were up-regulated in S4 leafy flowers (Liu et al., 2014). The SVP of Arabidopsis (AtSVP) is an MTF and functions as a negative regulator of floral development as part of a complex with FLOWERING LOCUS C (AtFLC) to control flowering time by negatively regulating *FLOWERING LOCUS T* (*AtFT*) and *SUPPRESSOR OF OVEREXPRESSION OF CONSTANS1* (*AtSOC1*) by directly binding their promoter sequences (Lee et al., 2007b; Li et al., 2008; Jang et al., 2009; Irish, 2010). Moreover, AtSVP also interacts with other components, such as AP1 and AGAMOUS-LIKE24 (AGL24), during stages 1 and 2 of flower development to repress floral homeotic genes that control petal, stamen, and carpel identity (Gregis et al., 2009). The *svp* mutant (*svp32*) of Arabidopsis exhibits an early-flowering phenotype, whereas constitutive expression of *AtSVP* in Arabidopsis delays flowering (Hartmann et al., 2000; Gregis et al., 2006; Lee et al., 2007a). Moreover, transgenic Arabidopsis expressing *AtSVP* orthologs from *Actinidia* spp. or rice (*Oryza sativa*) showed leaf-like sepals and secondary flower phenotypes (Trevaskis et al., 2007; Wu et al., 2012). In addition to MTF down-regulation, phytoplasma might induce leafy flower symptom development via up-regulated *SVP* expression.

MTF plays a role in the regulation of gene expression, whereas miRNA plays a role in posttranscriptional regulation. Whether phytoplasma effectors alter the miRNA expression levels for symptom development is an interesting question. MiRNAs regulate numerous transcription factors involved in plant development through RNA cleavage or translation inhibition (Kidner and Martienssen, 2005; Voinnet, 2009). In contrast to animal miRNAs, plant miRNAs display a high degree of sequence complementarity to their target mRNAs and guide cleavage of the target RNA via ARGONATUTE1 (AGO1; Kidner and Martienssen, 2005; Voinnet, 2009). In animals, the imperfect miRNA/target pairwise region results in translation inhibition and, consequently, decay

of the target mRNA (Bazzini et al., 2012; Djuranovic et al., 2012). However, the mechanism of translation inhibition in plants is not well known.

Chorostecki et al. (2012) proposed a predicted miR396 target site on the MADS box region of the *AtSVP* mRNA. Nevertheless, the lack of direct evidence from 5′ RACE data left them unable to demonstrate miR396-mediated *AtSVP* cleavage (Chorostecki et al., 2012). In contrast, the miR396-mediated *GROWTH-REGULATING FACTOR* (*AtGRF*) family of Arabidopsis features a bulge between the seventh and eighth positions of miR396 that is highly conserved among different plant species. The 5′ RACE data indicated that the bulge structure did not affect miR396-mediated *AtGRF* cleavage. However, interaction along the 5′ portion of the miRNA is the feature most relevant to its activity and cleavage efficiency (Mallory et al., 2004; Schwab et al., 2005; Lin et al., 2009), and modifying the pairing status of the 5′ portion of miR396 through mutagenesis alters the efficiency of *AtGRF2* cleavage (Debernardi et al., 2012). Moreover, Li et al. (2013) demonstrated that a 5′ miRNA mismatch triggers miRNA-mediated target RNA translation inhibition in Arabidopsis. These results suggest that mispairing of the 5′ portion of the miRNA plays a role in modulating cleavage efficiency and translation inhibition during target gene regulation.

We previously identified miR396 of *C. roseus* via whole-transcriptome analysis and small RNA profiling by next-generation sequencing (Chang, 2012; Liu et al., 2014). There are two mismatches in the 5′ portion of the miR396 (fourth and fifth positions) on the pairwise region of miR396/*CrSVPs* (Chang, 2012). Therefore, this study seeks to answer several questions: (1) whether *CrSVP1/2* are targets of miR396; (2) whether the regulation approaches differ between miR396/*CrSVPs* and miR396/*CrGRFs* due to the two mismatches in the 5′ portion of the miRNA; (3) whether the PHYL1 effector of PnWB also determines leafy flower phenotype in Arabidopsis; and (4) whether PHYL1 alters MTF and miRNA expression levels.

In this study, transgenic Arabidopsis expressing the *PHYL1* gene of PnWB (*PHYL1* plant) was generated and showed an identical leafy flower phenotype. The leafy flowers of *PHYL1* plants exhibited a lower miR396 expression level but higher *AtSVP* and *AtGRF1* expression levels compared with normal flowers of Columbia-0 (Col-0) plants. Moreover, we demonstrated that miR396 triggers *SVP* down-regulation via mRNA decay rather than cleavage based on degradome analysis. The mechanisms of PHYL1-altered miR396/*SVP* expression levels and miR396-mediated *SVP* down-regulation were investigated.

RESULTS

Abnormal Gene and miRNA Expression in PnWB-Infected *C. roseus*

Deep sequencing was used to compare the whole transcriptome with the small RNA profiles of *C. roseus*

HF and S4 PnWB-infected leafy flowers (Fig. 1A). The floral homeotic gene expression levels were compared between HF and S4 flowers. The expression levels of *CrFT*, *PISTILLATA* of *C. roseus*, *FOREVER YOUNG FLOWER* of *C. roseus*, *CrAP1.1*, *CrAP3.1*, and *CrAP3.2*, but not *CrAP1.2*, *CrSOC1.1*, and *CrSOC1.2*, which enhance flowering, were repressed in the S4 flowers (Fig. 1B). In contrast, the expression levels of *CrSVP1* and *CrSVP2* were increased in S4 flowers (Fig. 1B). *AGAMOUS* of *C. roseus* and *CrAP2* were not differentially expressed between HF and S4 flowers (Fig. 1B). In addition, we observed that most *C. roseus* miRNAs were significantly down-regulated in the S4 flowers, with only the up-regulation of miR162, miR169, and miR398 observed (Fig. 1C). These results suggest that PnWB effectors or other bacterial proteins might directly or indirectly alter either the miRNA gene expression profile of *C. roseus* plants (*CrMIR* genes) or the floral homeotic gene expression levels in PnWB-infected plants.

The PHYL1 Effector of PnWB Causes Leafy and Abnormal Flower Phenotypes and Represses miR396 Expression in Arabidopsis

The SAP54 effector of AYWB causes leafy flower in transgenic Arabidopsis (MacLean et al., 2011). We identified a *PHYL1* effector gene in the PnWB genome sequence (Chung et al., 2013) that shares 61.3% amino acid sequence similarity with AYWB and 56% similarity with PHYL1 of the onion yellows phytoplasma wild-type line (Fig. 2A) and determined whether PHYL1 of PnWB can cause leafy flower and alter miRNA expression. *PHYL1* plants, which overexpress the *PHYL1* of PnWB, exhibit two types of leafy flowers (Fig. 2B) and three types of abnormal flowers (Fig. 2C), depending on the severity of the abnormal phenotype in the flowers. The type I leafy flower phenotype exhibits sepal enlargement, petal shrinking, and stigma elongation (Fig. 2B). The type II leafy flower phenotype features a secondary flower growing out from the primary flower (Fig. 2B). In some cases, a cauliflower-like inflorescence with narrow interspaces and short pedicles results (Fig. 2B). Three types of abnormal flowers include asymmetric petals, abnormal petal, and stamen numbers (five to six petals and seven to eight stamens; AF-I), swollen stigma, and secondary flower growth (Fig. 2C). We assume that various phenotypes occurred on *PHYL1* plants because of the various expression levels of PHYL1.

Interestingly, in *PHYL1* and *SAP54* plants, most miRNAs were up-regulated compared with Col-0 plants, whereas miR156h, miR159, miR390, and miR396 were repressed, indicating that both effectors have similar functions in *CrMIR* gene regulation (Fig. 3A). However, PnWB infection inhibits most *CrMIR* genes (Fig. 1C). We hypothesize that the other effectors of PnWB might be involved in the repression of *CrMIR* genes. Furthermore, PHYL1 and SAP54 have specificity in the repression of particular miRNAs. Indeed, the northern-blot data also
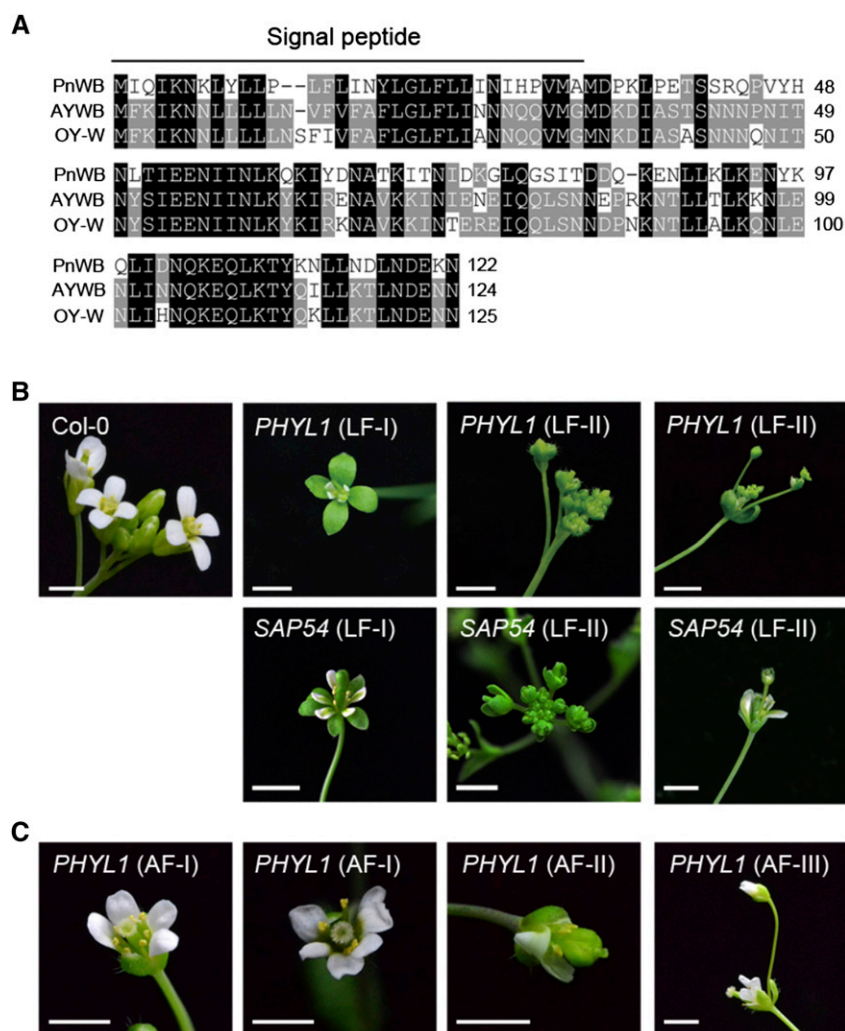
Figure 2. The phytoplasma effectors trigger the leafy flower phenotype. A, Alignment of orthologous amino acids of PHYL1. OY-W, Onion yellows phytoplasma wild-type line. B, Leafy flower phenotypes of *PHYL1* and *SAP54* plants. The type I leafy flower is indicated as LF-I, and the type II leafy flower is indicated as LF-II. Bars = 0.5 cm. C, The abnormal flower phenotype of *PHYL1* plants. The type I to III phenotypes are indicated as AF-I, AF-II, and AF-III, respectively. Bars = 0.5 cm.

indicated that the leafy flowers of *PHYL1* plants exhibited lower miR396 accumulation (0.57-fold) compared with Col-0 plants (Fig. 3B).

Identification of the *MIR396* Gene of *C. roseus*

The hairpin structures of the miR396 precursor of *C. roseus* (DDS44007) and its miRNA/miRNA* pairing positions are shown in Figure 4A. The miR396/miR396* duplex exhibits a two-nucleotide overhang at the 3′ end (Fig. 4A). Remarkably, 14,256 reads of the mature form of miR396 were obtained for the HF flowers, whereas only 1,482 reads of miR396* were obtained (Fig. 4A). These results satisfy the general rule that less miRNA* than the mature form of the miRNA is required in vivo because the miRNA* exhibits a rapid turnover rate due to cleavage by AGO1 (Guo and Lu, 2010). Importantly, the amount of miR396 was reduced (2,587 reds) in S4 flowers, which is consistent with previous observations (Fig. 4A). In addition, the complementary DNA (cDNA) of the miR396 precursor was cloned from the *C. roseus* flower

by reverse transcription (RT)-PCR for further investigation (data not shown), suggesting that the miR396 precursor exists in *C. roseus* plants.

The MADS Box Domain of the *SVP* Gene Contains a Potential miR396 Target Site

Based on sequence pairing, a putative miR396 target site was identified on the MADS box domain of the *SVPs* (Fig. 4B); however, the miR396-mediated cleavage of *SVP* was not confirmed by 5′ RACE (Chorostecki et al., 2012). The target sequences in *CrSVP1* and *CrSVP2* were highly conserved with that of *AtSVP* (AT2G22540) of Arabidopsis, and four mismatches (the fourth, fifth, 19th, and 20th positions of miR396) were identified in the pairwise region of miR396/*CrSVP1* or miR396/*AtSVP* (Fig. 4B). However, the pairwise region of miR396/*CrSVP2* had an extra G-to-A mismatch at the seventh position of miR396 (Fig. 4B).

MiR396 was down-regulated 0.06-fold in the S4 leafy flower compared with the HF (Fig. 4C). Moreover, semi-RT-PCR results indicated that the levels of

Figure 3. Phytoplasma effectors interfere with miRNA expression. A, MiRNA expression in flowers of Col-0, *PHYL1*, and *SAP54* plants as represented by a heat map. Red indicates up-regulated expression, and blue indicates down-regulated expression. The values at right indicate the results of the log₂ (Col-0/*PHYL1* or Col-0/ *SAP54*) formula. B, MiR396 detection in Col-0, *PHYL1*, and *svp32* plants by northern blot. U6 was used as a loading control. The numbers indicate the relative expression of miR396 compared with Col-0 plants.
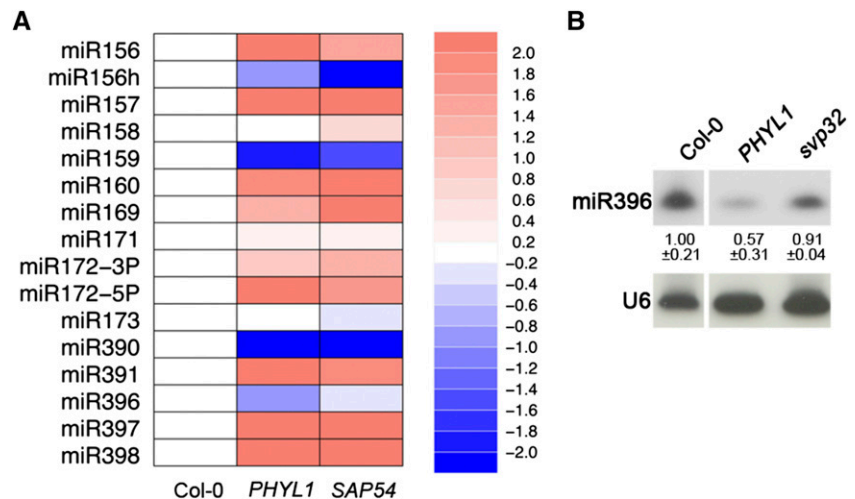
CrSVP1 were up-regulated 3.2- and 3.5-fold in the S4 leafy flower and healthy leaf samples, respectively, compared with the HF (Fig. 4D). In addition, *CrSVP2* was up-regulated 3.4- and 4.6-fold in S4 and healthy leaf, respectively (Fig. 4D). These data suggest that PnWB infection alters the expression of *CrSVP1/2* and miR396.

SVPs Contain Mismatch Pairings at the Target Site in the 5′ Portion of miR396

Alignment of the *SVP* genes revealed highly conserved miR396 target sites in various species. Fewer than five mismatches were observed on these *SVP*-miR396 pairwise regions, whereas 94% of MADS box genes had more than six mismatches spread throughout parallel regions of *AtSVP*, such as *AtAGL24* and *AtFLC* (Fig. 5A; Supplemental Fig. S1). The *AtGRF* gene family is also the target of miR396 (Jones-Rhoades and Bartel, 2004; Wang et al., 2004; Debernardi et al., 2012). However, the *AtGRF*-miR396 pairwise region exhibits mostly complementary pairing that differs from the *SVP*-miR396 pairing (Fig. 5B). Thus, we assume that the miR396-mediated degradation efficiency or approaches between miR396/*SVPs* and miR396/*AtGRFs* might differ (Fig. 5, A and B).

MiR396-Mediated Down-Regulation of *SVPs* by Transient Expression

Different concentrations of agrobacteria carrying the *MIR396a* gene of Arabidopsis (*AtMIR396a*) were transiently coexpressed with *AtSVP* in *Nicotiana benthamiana* plants and were then analyzed via agroinfiltration to evaluate whether miR396 can down-regulate *AtSVP*. The *AtSVP* gene was expressed using a Cauliflower mosaic virus 35S promoter to avoid the side effects of endogenous transcription factors that are regulated by miR396. The *AtSVP* RNA levels were decreased

by increasing miR396 expression levels (Fig. 5C). Similar results were observed for the miR396-mediated down-regulation of *CrSVP1*, *CrSVP2*, and *AtGRF1* (Supplemental Fig. S2). No *CrSVP1* down-regulation occurred when amiRGFP4 was present (an artificial miRNA that targets the *GFP* gene used as a negative control; Supplemental Fig. S3). These data indicate that miR396 directly triggers *SVP* posttranscriptional down-regulation.

To further demonstrate the target gene down-regulation by miR396, a reporter assay was used in this study. A DNA fragment (129 nucleotides in length) that contains a target site for *AtSVP* and *AtGRF1* was fused at the 5′ end of the *YELLOW FLUORESCENT PROTEIN* (*YFP*) gene to generate *SVP₁₂₉-YFP* and *GRF1₁₂₉-YFP* constructs, respectively (Fig. 6A). Moreover, *SVP₁₂₉ₘ-YFP* is a mutant construct that has several mutations at the target site, resulting in eight mismatches in the pairwise region of miR396 (Fig. 6A). The *SVP₁₂₉-YFP* and *GRF1₁₂₉-YFP* constructs resulted in an approximately 85% reduction of YFP fluorescence when these constructs were coexpressed with miR396, whereas no significant differences were observed regarding YFP fluorescence in the *YFP* negative control with/without miR396 (Fig. 6, B and C). In contrast, the *SVP₁₂₉ₘ-YFP* construct resulted in an approximately 40% reduction of YFP fluorescence when coexpressed with miR396 (Fig. 6, B and C). Notably, the fluorescent spots are present in nuclei (Fig. 6B). The reporter assay demonstrated that miR396 specifically down-regulated *AtSVP* and *AtGRF1*.

Flowering Phenotypes of miR396 in Loss and Gain of Function

We used genetic approaches to examine gain of function and loss of function in miR396-mediated *SVP* regulation. A transfer DNA (T-DNA) insertion mutant line, SALK064047, was demonstrated to be an *AtMIR396a* mutant (*atmir396a-1*) in Arabidopsis (Bao
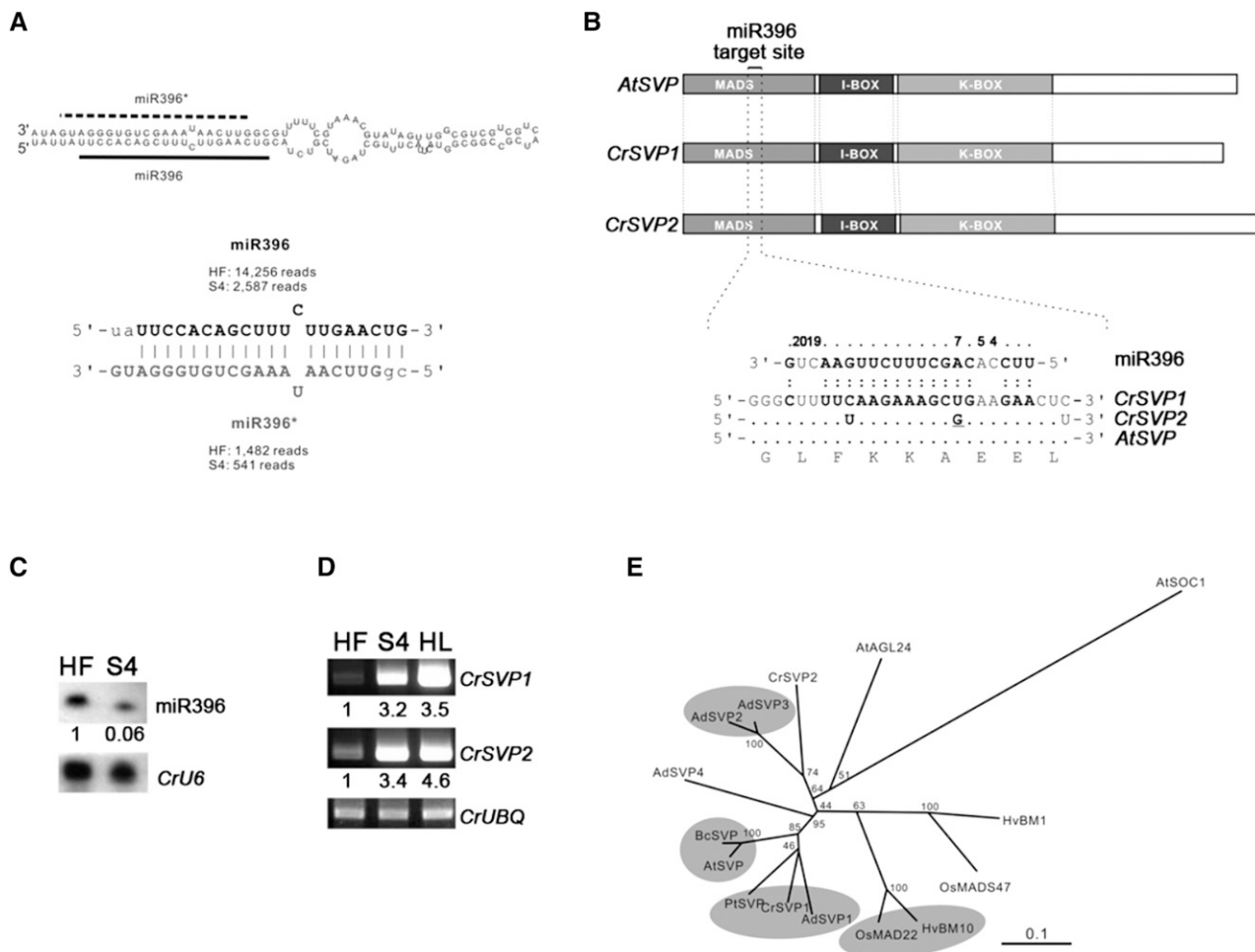
Figure 4. Characterization of *MIR396*, *CrSVP1*, and *CrSVP2* in *C. roseus*. A, Illustration of the hairpin structures of the *MIR396* precursors of *C. roseus* and their paired sequences. The mature miR396 (solid line) and miR396* (dashed line) are indicated on the precursor structure (top). The pairing of the miR396 (black) and miR396* (gray) sequences are indicated at bottom. The numbers indicate the deep-sequence reads of miR396 or miR396*. B, Predicted targets of miR396 in the MADS box domain of *SVP* genes. The nucleotide sequences of the *CrSVP1* (DDS_51524), *CrSVP2* (DDS_57797), and *AtSVP* (AT2G22540) targets were aligned, and the paired regions with miR396 are indicated. In the *SVP* alignment, dots indicate identical nucleotides, whereas boldface letters indicate the nucleotides that are perfectly paired between *SVP* and miR396. The translated SVP amino acids are presented below the alignment. C, Analysis of miR396 expression between HF and S4 PnWB-infected leafy flower by small RNA northern blot. The small RNA loading quantity was adjusted to 200 ng using the 2100 Bioanalyzer (Agilent). The numbers below indicate the relative fold change in the expression of miR396 regarding the S4 flowers relative to the HFs. *CrU6* small nuclear RNA was used as a loading control. D, Semi-RT-PCR analyses of the *CrSVP1* and *CrSVP2* expression levels in an HF, S4 flower, and healthy leaf (HL). *UBIQUITIN* (*UBQ*) of *C. roseus* was used as an internal control. The numbers indicate the fold change in *CrSVP1* and *CrSVP2* expression in the S4 flower and HL samples relative to the HF. E, Phylogenetic tree of SVP proteins. The genes sharing greater than 80% amino acid similarity are classified and shaded in gray. AtSOC1 is referred to as an outgroup. The numbers indicate the percentage of 1,000 bootstrap replicates at the appropriate nodes. The scale bar indicates a 0.1 divergence of amino acid substitutions per site.

et al., 2014). T-DNA was inserted at the −450-bp promoter region of *AtMIR396a* (AT2G10606; Fig. 7A). The homozygous *atmir396a-1* plants exhibited only 0.6-fold miR396 expression levels compared with Col-0 plants (Fig. 7B). We assumed that this expression represents a background signal of miR396b in *atmir396a-1* plants (Fig. 7B). The *atmir396a-1* plants exhibit normal flower and flowering time phenotypes, whereas the *svp32* plants display early flowering (Fig. 7, C and D). In addition, *atmir396a-1* plants exhibit 0.5- and 0.3-fold increased *AtSVP* and *AtGRF1* expression, respectively, compared with Col-0 plants (Fig. 7E), indicating that lower miR396 levels induce up-regulation of *AtSVP* and *AtGRF1*.

In contrast, transgenic Arabidopsis expressing *CrMIR396* (*CrMIR396* plant) exhibits abnormal flowers with curved sepals and petals and enlarged stigmas, consistent with transgenic Arabidopsis expressing
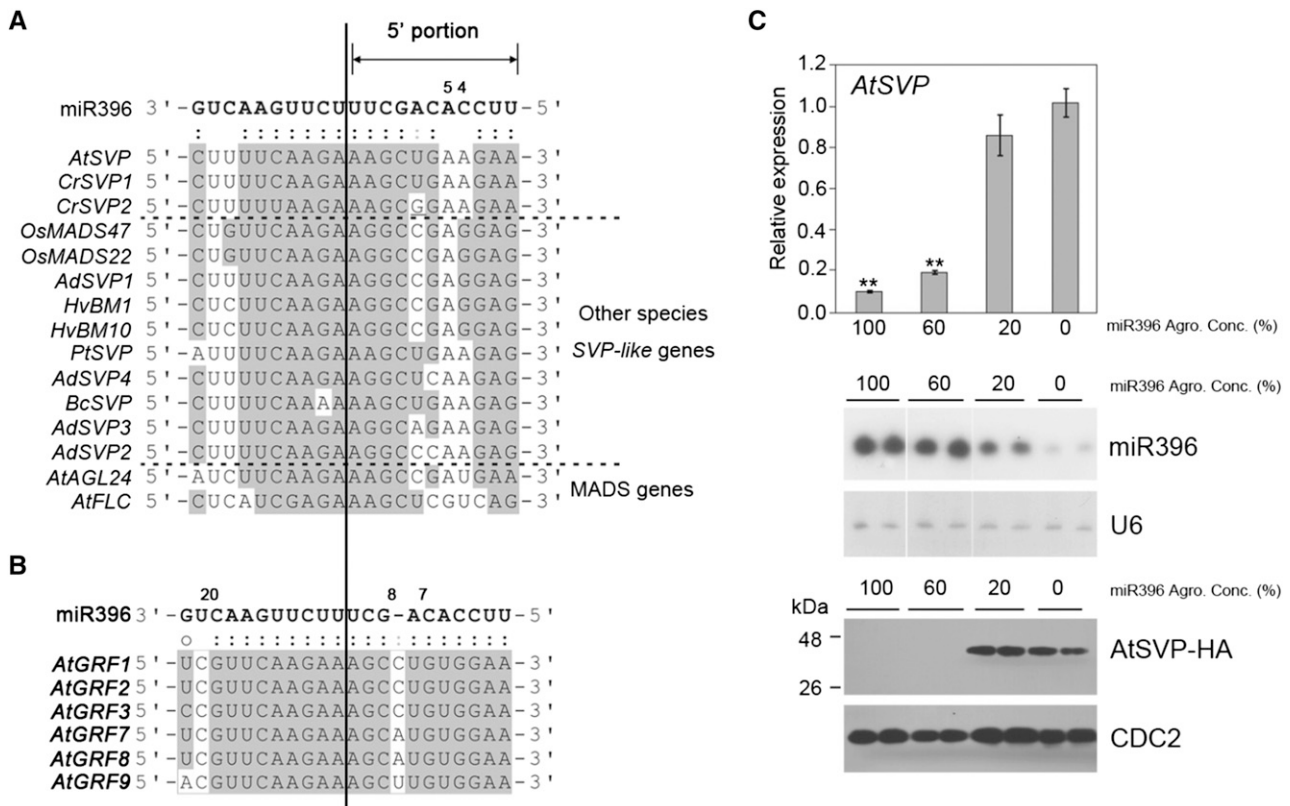
Figure 5. *SVP* contains variation pairing of the 5′ portion of miR396 with its target genes. A, Highly conserved miR396 target sites on the *SVP* genes of various species. The alignment of the miR396 target sites in *SVP* genes of various species is shown. The GenBank accession numbers of the *SVP* genes are as follows: *AtSVP* (NM127820), *AtAGL24* (NM118587), *AdSVP1* (JF838212), *AdSVP2* (JF838213), *AdSVP3* (JF838214), *AdSVP4* (JF838215), *HvBM1* (AJ249142), *HvBM10* (EF043040), *OsMADS22* (AB107957), *OsMADS47* (AY345221), *BcSVP* (DQ922945), and *PtSVP* (FJ373210). *AtAGL24* and *AtFLC* (AT5G10140) were chosen as representative *MADS* genes for target-site comparison. The *SVP* nucleotides that pair with the miR396 sequences are indicated in gray. B, The miR396 target-site alignment for *GRFs* (*AtGRF1*, AT2G22840; *AtGRF2*, AT4G37740; *AtGRF3*, AT2G36400; *AtGRF7*, AT5G53660; *AtGRF8*, At4G24150; and *AtGRF9*, AT2G45480). Gray shading indicates the nucleotides of *AtGRFs* paired with the miR396 sequences. C, In vivo analysis of miR396-mediated *AtSVP-HEMAGGLUTININ* (*HA*) efficiency by transient expression. The relative expression levels of *AtSVP* were normalized to that of *NbACTIN* via real-time RT-PCR. Error bars represent SE ($n = 6$). The relative expression levels were significantly different from those in Col-0 plants for each RNA sample, based on Student's *t* test: **, $P < 0.01$. The various percentages of miR396 were determined by a small RNA northern blot. U6 small nuclear RNAs were used as loading controls. The various percentages of miR396 are indicated below the real-time RT-PCR and northern-blot data. The AtSVP-HA protein level was detected by western blotting with a 1:10,000 dilution of HA antibody. *CELL DIVISION CONTROL2* (*CDC2*) was used as a protein loading control.

AtMIR396a (*AtMIR396a* plant; Fig. 7C; Liang et al., 2014). Two individual *CrMIR396* plants (lines 8 and 27) exhibited 4.6- and 3.5-fold increased miR396 expression compared with Col-0 plants. Furthermore, *AtMIR396a* plants exhibited a 1.9-fold increase in miR396 expression (Fig. 7B). *CrMIR396* and *AtMIR396a* plants exhibited late-flowering phenotypes that were correlated with the expression levels of miR396 (Fig. 7D). Moreover, *AtSVP* and *AtGRF1* were down-regulated in *CrMIR396* and *AtMIR396a* plants (Fig. 7E). *AtGRF1* was down-regulated by more than 80% by the overexpression of miR396, while *AtSVP* was downregulated by only 20% to 40% in *MIR396* plants (Fig. 7E). These results indicated that *CrMIR396* can generate miR396 and has a genetic function similar to that of *AtMIR396a* in Arabidopsis plants. Moreover,

miR396 regulates *AtGRF1* more efficiently than *AtSVP*.

SVP Orthologs from Different Species Cause Various Flower Phenotypes

Two orthologous *SVP* genes (*CrSVP1* and *CrSVP2*) from *C. roseus* were overexpressed in Arabidopsis (*CrSVP1* and *CrSVP2* plants), and transgene overexpression was confirmed by RT-PCR (Supplemental Fig. S4). However, both plants exhibited normal flower phenotype and flowering time (Fig. 7, C and D). In addition, transgenic Arabidopsis expressing the *SVP2* gene of *Actinidia* spp. (*AdSVP2* plants) exhibited enlarged sepals, small green petals, and a curving pistil
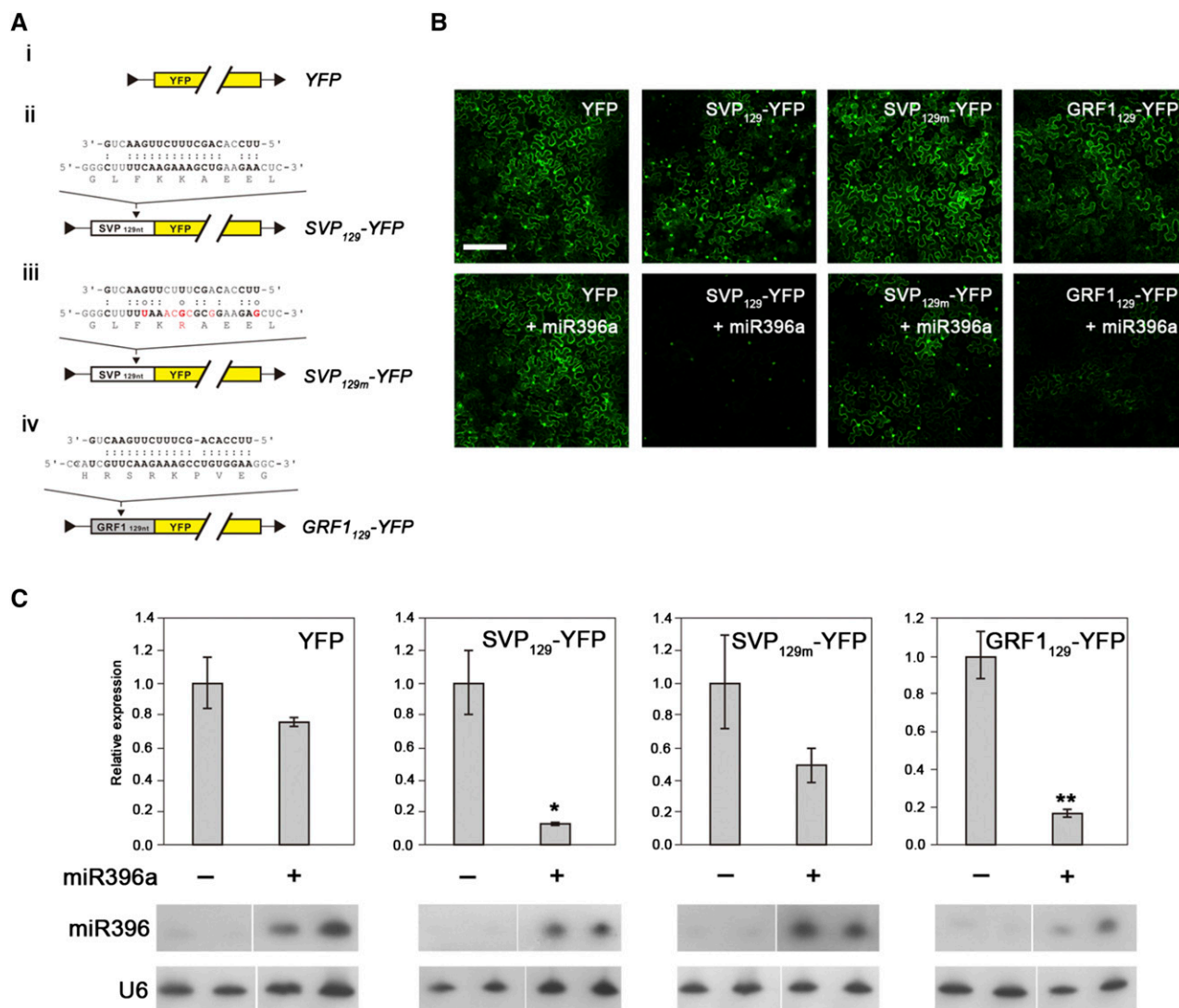
Figure 6. The reporter assay for miR396-mediated targeted down-regulation. A, Schematic of miR396 and its target-site pairing on the *YFP* gene. All of the constructs were constructed on a binary vector under the control of a 35S promoter. A *YFP*-only construct (i) was used as a negative control. The SVP_{129}-*YFP* construct (ii) represents 129 nucleotides of the 5′ end of the *SVP* gene containing the miR396 target site fused with the *YFP* gene. The SVP_{129m}-*YFP* construct (iii) represents 129 nucleotides of the 5′ end of the *SVP* gene containing a mutated miR396 target site fused with the *YFP* gene. The $GRF1_{129}$-*YFP* construct (iv) represents 129 nucleotides of the 5′ end of the *GRF1* gene containing the miR396 target site fused with the *YFP* gene. B, The YFP reporter assay was analyzed using confocal microscopy. Bar = 100 μm. C, Relative average YFP expression levels ($\log_2$) of the reporter assay as determined by confocal microscopy ($n = 3$). Relative YFP expression levels were significantly different from that of the negative control construct without miR396 present in each sample, based on Student's *t* test: **, $P < 0.01$; and *, $P < 0.05$. MiR396 was detected by northern blot for each sample (two replicates). U6 small nuclear RNA was used as a loading control.

mimicking the leafy flower phenotype of *PHYL1* plants (Fig. 7C); however, the flowering time of the *AdSVP2* plant was similar to that of Col-0 plants (Fig. 7D). In contrast, the *AtSVP* plants showed asymmetric petals of an abnormal flower phenotype identical to *PHYL1* plants (Figs. 2C and 7C). In some cases, the severely abnormal flowers of *AtSVP* plants had five petals with eight stamens (Fig. 7C). These data suggested that the up-regulation of *AtSVP* causes an abnormal flower phenotype. The abnormal flower

phenotype in *AtSVP* plants is consistent with the AF-I of PHYL1 plants, which have five to six asymmetric petals and seven to eight stamens (Figs. 2C and 7C).

Two individual lines of *AtSVP* plants (lines 1 and 2) exhibited late flowering time with 16 to 19 rosette leaves. Indeed, phylogenetic analysis revealed that AtSVP, AdSVP2, CrSVP1, and CrSVP2 are in different groups based on 80% amino acid similarity (Fig. 4E). Moreover, the C-terminal regions of these SVPs differ (Supplemental Fig. S5). These results imply that the
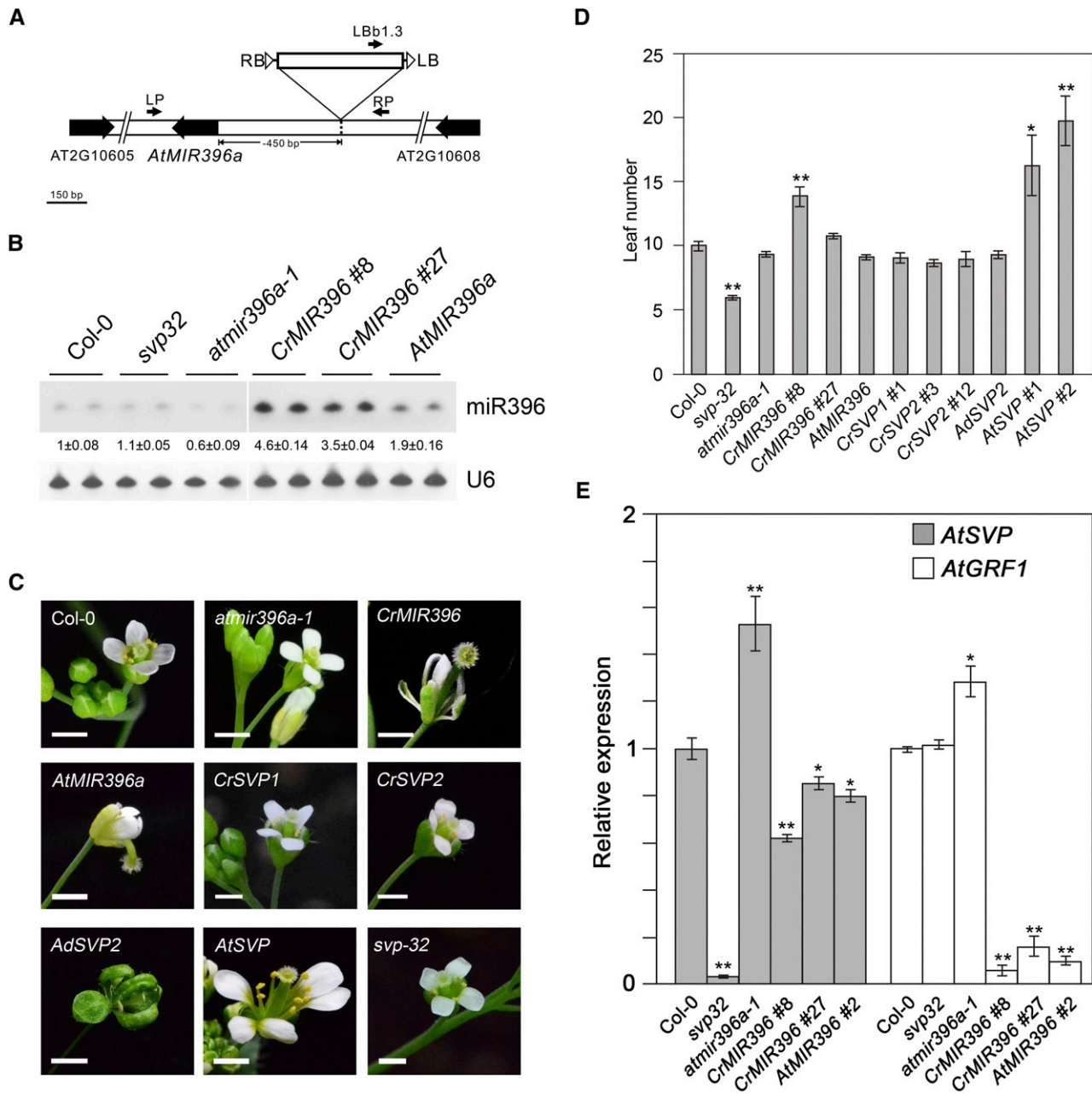
Figure 7. Characterization of miR396 and *SVPs* in Arabidopsis plants. A, Diagram of the *atmir396a-1* mutant (SALK064047). The black arrows indicate the gene regions for AT2G10605, *AtMIR396a* (AT2G10606), and AT2G10608 and their translation directions. The T-DNA insertion site is located at the promoter region (450 bp upstream) of *AtMIR396a*. The left border (LB) and right border (RB) are indicated at the two borders of the T-DNA. The primers LP, RP, and LBb1.3 were used for genotyping via PCR. Bar = 150 bp. B, Analysis of miR396 by small RNA northern blot in Col-0, *svp32* mutant, *atmir396a-1* mutant, two in-dependent *CrMIR396* lines (lines 8 and 27), and *AtMIR396a*-overexpressing plants. U6 small RNA was used as a loading control. The numbers below indicate fold changes in miR396 expression relative to the Col-0 plant. C, *CrSVP1*, *CrSVP2*, *atmir396a-1*, and *svp32* (SALK072930C) mutant plants exhibited normal flower phenotypes. *CrMIR396* and *AtMIR396a* plants exhibited abnormal flower phenotypes. Plants with *AdSVP2* or *AtSVP* overexpression exhibited leafy or abnormal flower phenotypes, respectively. Bars = 0.1 cm. D, Evaluation of the flowering time of various Arabidopsis mutant or transgenic plants. Leaf number represents flowering time. Error bars represent SE (*n* = 20). E, MiR396-mediated *AtSVP* and *AtGRF1* regulation. *AtSVP* and *AtGRF1* were detected by real-time RT-PCR. Relative expression levels were normalized to the level of *AtUBQ*. Error bars represent SE (*n* = 3). Relative expression levels were significantly different from those of the Col-0 plants in each RNA sample, based on Student's *t* test: *, *P* < 0.05; and **, *P* < 0.01.

SVP genes in other species have functions regarding flower phenotypes and flowering times that differ from those in Arabidopsis. In addition, the abnormal flower phenotypes in *AdSVP2* and *AtSVP* plants suggest that overexpression of *SVP* may alter flower development. To confirm this hypothesis, *AtSVP* expression was detected in *PHYL1* plants.

SVP Is Up-Regulated in the Sepal and Petals of *PHYL1* Plants

Because miR396 expression was reduced in *PHYL1* plants, we evaluated *AtSVP* and *AtGRF1* expression in transgenic plants. Real-time RT-PCR analysis revealed that *AtSVP* and *AtGRF1* are up-regulated in the *PHYL1* leafy flower (Fig. 8A). Moreover, in situ hybridization data indicate strong accumulation of *AtSVP* signals in the leafy flower tissue of *PHYL1* plants, particularly in the basal part of the petals (Fig. 8B, image ii), whereas few *AtSVP* signals were observed in the sepals of Col-0 plants (Fig. 8B, image i). The sense probe for *AtSVP* was used as a negative control for in situ hybridization, and no signal was observed in flower buds of *PHYL1* or Col-0 plants (Fig. 8B, images iii and iv). These results support the hypothesis of miR396-mediated *AtSVP* expression in flower tissue.

MiR396 Triggers *SVP* Decay

The pairwise fourth and fifth positions are reportedly critical for the efficiency of low miRNA-guided cleavage of the target RNA (Lin et al., 2009). We assumed that the two mismatches at the fourth and fifth positions of the pairwise region will yield differences in cleavage between miR396/*AtSVP* and miR396/*AtGRF1*. To test this

hypothesis, a high-throughput degradome approach was used to analyze the mRNA degradation products. Overexpression of miR396 yielded 22,705 degradome reads of degraded 3' *AtGRF1* fragments in the *CrMIR396* plant, whereas only 800 degradome reads were obtained from Col-0 plants (Fig. 9A). In addition, 3,744 degradome reads of *AtGRF1* were obtained from *EXORIBONUCLEASE4* mutant (*xrn4-5*), a 5'-to-3' exoribonuclease mutant, whereas approximately 500 degradome reads were detected in *SAP54* plants (Fig. 9A). These data indicate that miR396-mediated *AtGRF1* cleavage is dependent on miR396 dosage and that the cleaved 3' *AtGRF1* fragment is highly accumulated in *xrn4-5* mutants. A 3- to 5-fold increase in *AtGRF1* degradome reads was detected in *CrMIR396* and *xrn4-5* plants compared with Col-0 plants (Fig. 9B). In addition, the other *AtGRF* targets, Arabidopsis *BASIC HELIX-LOOP-HELIX74* (AT1G10120) and *AtMMG4.7* (AT5G43060), which are also targets of miR396, also produced significant degradome reads on the corrected target site (Supplemental Fig. S6). These results indicate that miR396 mediated *AtGRF1* cleavage at the target site.

While no degradome reads were detected for the target site of *AtSVP* in these plants, approximately 280 various degradome reads were identified at the rear position of the miR396 target site in *CrMIR396* plants, suggesting the presence of miR396-mediated *AtSVP* decay (Fig. 9C, white arrowheads). Total degradome reads of *AtSVP* were increased 5-fold in *CrMIR396* plants compared with Col-0 plants, but no significant reads were detected in either *xrn4-5* or *SAP54* plants (Fig. 9C). Identical results were obtained for the degradome profile of *C. roseus* flowers (Fig. 9E, images i and ii). In total, 52 and 21 degradome reads were detected for the rear positions of the target sites on
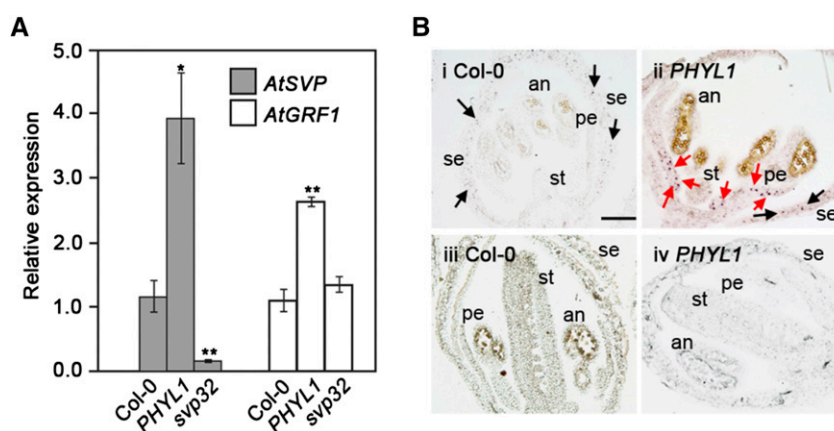

Figure 8. PHYL1 alters the expression of miR396 and its targets. A, *AtSVP* and *AtGRF1* expression levels in Col-0, *PHYL1*, and *svp32* plants were detected by real-time RT-PCR. Error bars represent SE (*n* = 9). Relative expression levels were normalized to the level of *AtUBQ*. Relative expression levels were significantly different from those of the Col-0 plants in each RNA sample, based on Student's *t* test: *, *P* < 0.05; and **, *P* < 0.01. B, Detection of *SVP* gene expression in floral bud tissue by in situ hybridization. The buds of Col-0 (i) and *PHYL1* (ii) plants were sectioned and hybridized with an antisense probe for *SVP* detection. The sense probe for *AtSVP* was used as a negative control (iii and iv). The black arrows indicate the *AtSVP* signal at the sepal, and the red arrows indicate the *AtSVP* signals at the basal part of the petal. an, Anther; pe, petal; se, sepal; st, stigma. Bar = 50 μm.
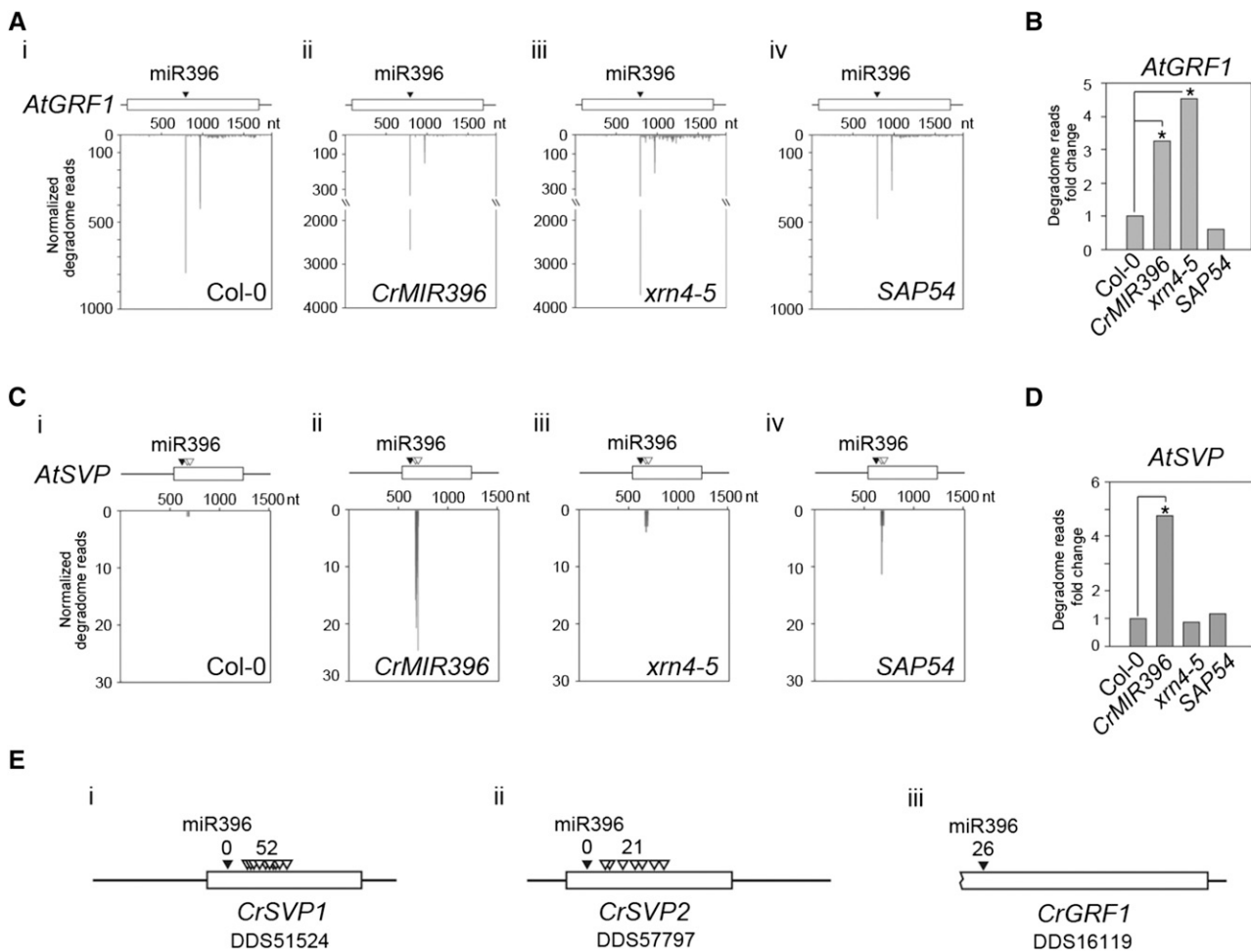
Figure 9. Degradome analysis of *C. roseus* and Arabidopsis. A and C, Degradome patterns of *AtGRF1* (A) and *AtSVP* (C) in flower buds of Col-0, *CrMIR396*, *xrn4-5* mutant, and *PHYL1* plants. nt, Nucleotides. B and D, Fold changes in the degradome of *AtGRF1* (B) and *AtSVP* (D) in flower buds of Col-0, *CrMIR396*, *xrn4-5* mutant, and *PHYL1* plants. The fold changes were significantly different from those of the Col-0 plants in each RNA sample based on Student's *t* test: *, *P* < 0.01. E, Degradome patterns of *CrSVP1*, *CrSVP2*, and *CrGRF1* in flowers of *C. roseus*. The black arrowheads indicate the miR396 target site. The white arrowheads indicate the nonspecific RNA degradation position.

CrSVP1 and *CrSVP2*, respectively, suggesting the presence of miR396-mediated *CrSVP1/2* decay. In contrast, 26 degradome reads of *CrGRF1* were detected in the target position, indicating miR396-mediated cleavage (Fig. 9E, image iii, black arrowhead). In addition, one predicted miR396 target gene (AT1G71350) exhibits mismatch pairing at the 5′ portion (Supplemental Fig. S7). No significant miR396-cleaved degradome reads at the target site were observed for the gene. However, AT2G31880 has approximately 5-fold more degradation reads in *CrMIR396* plants (Supplemental Fig. S7, B and C). In contrast, under the miR396-decreasing condition, AT2G31880 expression was increased 50% in *SAP54* plants, which suggests the presence of miR396-mediated AT2G31880 down-regulation (Supplemental Fig. S7D). In summary, based on the 5′ portion pairing differences between miR396 and its targets, miR396-mediated *SVP* or AT2G31880 down-regulation might differ from the

GRF1 control. In addition, this phenomenon is conserved in various plant species.

DISCUSSION

Multifunctional effectors are common in many pathogens. In addition to MTF degradation, we demonstrated that PHYL1 effector can up-regulate *SVP* MTF expression and alter miRNA expression to switch the phase transition back to the vegetative stage. In addition, we also provided evidence to show that miR396 mediated *SVP* mRNA decay.

The Effectors of PnWB Alter Gene and miRNA Expression in Host Plants

The virescence and phyllody symptoms on phytoplasma-infected plants are remarkable phenotypes. Phytoplasma

infection alters the physiological and morphological characteristics of the host cells to enhance pathogenic multiplication and infection in the *C. roseus* plants (Sugio et al., 2011). To revert the reproductive stage to the vegetative stage, PHYL1/SAP54 effectors suppress positive regulators of flowering but enhance the expression levels of negative regulators, such as *CrSVP1* and *CrSVP2*. However, *CrSOC1.1*, *CrSOC1.2*, and *CrAP1.2*, the orthologs of which function as positive regulators in flowering in Arabidopsis, were not repressed by PnWB. This phenomenon can be explained by two forces that originate from the pathogen and host to counteract each other; they are abnormally coexpressed in the floral meristem, resulting in leafy flower formation (Liu et al., 2014).

Rather than altering gene expression, the miRNA expression levels were also altered during PnWB infection. Interestingly, the miRNA expression patterns in PnWB-infected S4 leafy flowers differ in *PHYL1* and *SAP54* plants. We hypothesize that the other effectors or bacterial proteins in PnWB directly or indirectly control *CrMIR* gene expression, resulting in different miRNA expression patterns between PnWB-infected plants and transgenic plants. Moreover, the PHYL1/SAP54 that triggers MTF degradation might alter abnormal miRNA expression to cause a synergistic effect, thereby resulting in the leafy flower phenotype.

Like *SAP54* or *PHYL1* of onion yellows phytoplasma mutant plants, PHYL1 of PnWB effector causes leafy flowers in transgenic Arabidopsis plants. Moreover, the miRNA expression patterns of *PHYL1* plants (PHYL1 of PnWB) were also consistent with those of *SAP54* plants. SAP54 and PHYL1 of onion yellows phytoplasma plants mediate AtAP1, AtSEP3, and AtCAL proteasomal degradation (MacLean et al., 2014; Maejima et al., 2014); therefore, MTF degradation might result in abnormal miRNA expression. These results indicate that these effectors contain common motif(s) for triggering leafy flower formation and altering miRNA expression. Furthermore, PHYL1 mediates the down-regulation of miR396 expression; however, it did not interfere with miR396 biogenesis in vivo. PHYL1 might trigger MTF degradation or alter the expression levels of other factors that regulate miR396 expression.

In addition, the *atmir396a-1* mutant exhibited *AtSVP* accumulation without manifesting any abnormal flower phenotype. Our explanation for this observation is that the functional redundancy of miR396b might play a role in regulating *AtSVP*. Moreover, the 0.5-fold accumulation of *AtSVP* relative levels in *atmir396a-1* plants might not be sufficient to trigger the abnormal flower phenotype, whereas the 3- and 90-fold accumulation of *AtSVP* in *PHYL1* and *AtSVP* plants, respectively, might trigger this phenotype (Fig. 8; Supplemental Fig. S4B). In contrast, *AtMIR396a* and *CrMIR396* plants did not show the same early-flowering phenotype as the *svp32* mutant, possibly because miR396 also regulates other genes; therefore, the synergistic effect resulted in a milder late flowering.

The 5′ Portion of miR396 Determines Target RNA Degradation by miRNA Cleavage or mRNA Decay

The degradome patterns indicated that miR396-mediated *SVP* and *GRF1* degradation profiles differ because of the discrepant pairing on the 5′ portion of the miRNA. The 5′ portion (i.e. the fourth and fifth positions) of the miRNA is critical for miRNA-mediated cleavage, whereas the 19th and 20th positions are nonessential (Lin et al., 2009). The 5′ mismatch of miRNA reduces the efficiency of target RNA cleavage and may trigger mRNA decay (Lin et al., 2009; Bazzini et al., 2012; Djuranovic et al., 2012), which may explain the failure to confirm the miR396 target site of *SVP* by 5′ RACE (Chorostecki et al., 2012). Indeed, the degradome profiles showed that *CrSVP1*, *CrSVP2*, and *AtSVP* have nonspecific mRNA decay, whereas a clear degradome pick was shown on the target site of *CrGRF1* and *AtGRF1*. In miRNA regulation of mRNA by translation repression in animal models, miRNA-mediated silencing complex bound of mRNA is typically degraded by another endogenous RNase system (Stefani and Slack, 2008; Bazzini et al., 2012; Djuranovic et al., 2012). In plants, the miR398-mediated cleavage of the *COPPER/ZINC SUPEROXIDE DISMUTASE* (*CSD1* and *CSD2*) family, which exhibits a mismatch at the fourth position of miR398, demonstrated that miR398 regulates *CSD2* expression through translation repression (Sunkar et al., 2006; Li et al., 2013). Therefore, we hypothesize that *SVP* mRNA decay might be triggered by miR396-mediated translation inhibition.

PHYL1-Mediated MTF Degradation Might Interfere with the Heterodimer Formation of the SVP Complex

PHYL1/SAP54 interacts with the RAD23 family to trigger MTF (AP1, SEP3, and CAL) degradation,
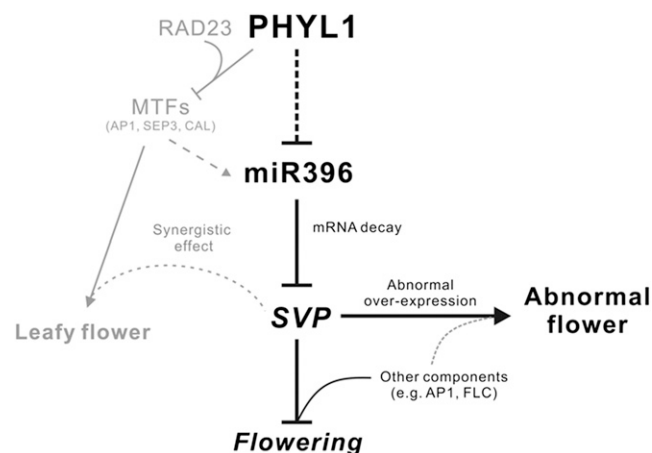

Figure 10. Model for PHYL1-regulated miR396-mediated *SVP* expression in the flowering pathway resulting in the abnormal flower phenotype.

resulting in the formation of leafy flower phenotypes (MacLean et al., 2014; Maejima et al., 2014). However, AtSVP interacts with AP1 or other components to form different complexes that regulate floral gene expression (Gregis et al., 2009). Therefore, the lack of AP1 in *PHYL1/SAP54* plants might prevent AtSVP from forming a heterodimer complex, thereby resulting in misregulation during the phase transition and floral organ identity. In addition, the degrees of phyllody and virescence of *SAP54* plants in the *rad23* family mutant background were reduced, especially in the *rad23BCD* triple mutant that has no strong leafy flower formation in the presence of phytoplasma infection or *SAP54* overexpression (MacLean et al., 2014). Interestingly, *rad23BCD* mutant plants have shown the abnormal flower (five to six petals) phenotype (MacLean et al., 2014) identical with the AF-I of *PHYL1* and *AtSVP* plants. Therefore, these data implied that the gain of function of the AtSVP-AP1 complex might also affect flower formation, while AP1 shows no degradation in the *rad23BCD* mutant background (Fig. 10). In addition, the SVP complex has species specificity with regard to interference with flowering time and flower development in Arabidopsis, because only *AtSVP* plants show the late-flowering and AF-I phenotypes in Arabidopsis, whereas other *SVP* plants have normal flowering time and normal flowers (except *AdSVP* plants), similar to Col-0 plants.

A Working Model for PHYL1 Repression of miR396-Mediated *SVP* Regulation

We propose a model for PnWB repression of the miR396-mediated *SVP* silencing pathway (Fig. 10). Multiple functions of PHYL1 trigger positive regulators of MTF (AtAP1, AtSEP3, and AtCAL) proteasomal degradation, resulting in leafy flower formation. PHYL1-mediated MTF degradation also affects many floral homeotic gene expression levels and miRNA expression levels, including the up-regulation of *AtSVP* and the repression of miR396. MiR396 regulates *SVP* through an mRNA decay approach that might be triggered by translation inhibition. Therefore, the down-regulation of miR396 by PHYL1 results in the up-regulation of *SVP* to change the complex formation to repress flowering and cause an abnormal flower phenotype.

CONCLUSION

This study provides evidence to demonstrate that PHYL1/SAP54 effectors can change miRNA expression levels. In addition, we also demonstrate that miR396 can down-regulate *SVP*, and the overexpression of *AtSVP* causes the abnormal flower phenotype. In the future, we will explore how PHYL1 controls these miRNA gene expression levels and examine symptom development with regard to the pathogen effector-host factor interaction at the posttranscriptional level.

MATERIALS AND METHODS

Plant Materials and Phytoplasma Infection

Arabidopsis (*Arabidopsis thaliana*) seeds were surface sterilized and chilled at 4°C for 2 d prior to sowing on Murashige and Skoog (MS) medium with or without suitable antibiotics for selection. One-week-old seedlings were germinated on MS plates and transferred to soil. *Catharanthus roseus* and *Nicotiana benthamiana* seeds were sown in soil. All seedlings and plants were maintained in a growth chamber or greenhouse (16 h of light/8 h of dark, 20°C–25°C).

Two-month-old *C. roseus* plants were inoculated with PnWB phytoplasma via grafting. The PnWB-infected plants developed virescence symptoms 3 to 4 weeks post grafting, whereas phyllody symptoms developed at 5 to 6 weeks post grafting.

Screening of *atmir396a* Mutants of Arabidopsis

Mutant lines of *atmiR396a-1* (SALK064047) for T-DNA insertion were obtained from The Arabidopsis Information Resource (http://www.arabidopsis.org/). Genomic DNA from 1-week-old seedlings was used for genotyping. The primers LP and RP were used to detect the wild-type genome region of the *AtMIR396a* gene, whereas the primers LBb1.3 and RP were used to detect the T-DNA insertion region. The primers used for genotyping are listed in Supplemental Table S1.

Gene Construction and Transgenic Plants

The genes *AtSVP*, *CrSVP1*, *CrSVP2*, *AtMIR396a*, *CrMIR396*, and PnWB *PHYL1* were identified based on the Arabidopsis (The Arabidopsis Information Resource) and *C. roseus* transcriptome databases (Chang, 2012; Liu et al., 2014). *AtSVP* was cloned via RT-PCR amplification using the primers F-AtSVP and R-AtSVP. For *AtGRF1*, the 5′ end of *AtGRF1* (792 nucleotides) was cloned via RT-PCR amplification using the primers F-AtGRF1 and R-AtGRF1-792. *CrSVP1* was cloned via RT-PCR amplification using the primers 51524_F and 51524_R. *CrSVP2* was cloned via RT-PCR amplification using the primers 57797_F and 57797_R. *AtMIR396a* was cloned via RT-PCR amplification using the primers F-AtMIR396a and R-AtMIR396a. *CrMIR396* was cloned via RT-PCR amplification using the primers 34004-29-F and 34004-235-R. The *PHYL1* gene was identified from the PnWB genome sequence (Chung et al., 2013) and amplified from the cDNA of PnWB-infected *C. roseus* by RT-PCR with the primers FG-PHYL1-Pn and RG-PHYL1-Pn. PCR fragments were cloned into the pENTR/D-TOPO vector (Invitrogen) according to the manufacturer's instructions to generate pENTR-CrSVP1, pENTR-CrSVP2, pENTR-CrMIR396, and pENTR-PHYL1.

For the miR396 target-site mutation of *AtSVP*, the *AtSVP* cDNA was used as a template for PCR-based mutagenesis with MAtSVPm2-118 and PAtSVPm2-70. The PCR fragments were cloned into pENTR/D-TOPO vector to generate pENTR-AtSVPm.

For the reporter assay, the *AtSVP*$_{129}$ and *AtSVP*$_{129m}$ DNA fragments (nucleotides 1–129 of the 5′ end of either *AtSVP* or *AtSVPm*) were amplified by PCR from pENTR-AtSVP as well as pENTR-AtSVPm with F-AtSVP and MAtSVP-129 primers. In addition, the *GRF1*$_{129}$ DNA fragment was amplified by PCR from pENTR-AtGRF1 with PAtGRF1-731 and MAtGRF1-817 primers. These PCR fragments were cloned into the pENTR/D-TOPO vector to generate pENTR-AtSVP$_{129}$, pENTR-AtSVP$_{129m}$, and pENTR-AtGRF1$_{129}$. Gateway system procedures were used to transfer these genes to a pBA-DC-YFP binary vector to generate pBA-AtSVP$_{129}$-YFP, pBA-AtSVP$_{129m}$-YFP, and pBA-AtGRF1$_{129}$-YFP.

These binary plasmids were transformed into an *Agrobacterium tumefaciens* ABI strain for agroinfiltration or used for transgenic Arabidopsis transformation using a floral dip procedure (Zhang et al., 2006). The transformant lines were screened on MS medium containing 10 μg mL^{-1} Basta (Sigma).

The artificial miRNA precursor that targets the *GFP* gene (*preamiR-GFP4*) was constructed based on the miR159 precursor of Arabidopsis via PCR mutagenesis using the primers PamiR-FG and MamiR. The PCR product was cloned into a pENTR/D-TOPO vector to generate pENTR-amiR-GFP4. Gateway system procedures were used to transfer *preamiR-GFP4* to a pBA-DC-HA binary vector (Zhang et al., 2005) and generate pBA-amiR-GFP4. The primers used for cloning are listed in Supplemental Table S1.

Transient Expression via Agroinfiltration

An *A. tumefaciens* ABI strain-containing binary vector was incubated in Luria-Bertani medium containing 10 mM MES, pH 5.6, 40 μM acetosyringone,

100 μg mL^{-1} spectinomycin, and 50 μg mL^{-1} kanamycin at 28°C for 16 h. The *A. tumefaciens* was suspended, the absorbance was adjusted to optical density at 600 nm = 0.5 using an appropriate buffer (10 mM MgCl$_2$ and 150 μM acetosyringone), and the *A. tumefaciens* was incubated at room temperature for 3 h (Lin et al., 2013). Four days after agroinfiltration, the infiltrated leaves of the *N. benthamiana* plants were collected and analyzed by semi-RT-PCR and northern blot.

For the observation of reporter assay results, YFP fluorescence in the infiltrated leaf was monitored using the Leica TCS SP5 II confocal laser-scanning microscope (Joint Center for Instruments and Research, College of Bioresources and Agriculture, National Taiwan University) equipped with a multiline argon laser with a filter set for YFP fluorescence (excitation filter, Acousto-optic Tunable filter 488; emission bandwidth, 496 to 574 nm; PMT2 offset [−1]/gain [895]). All images were graphically arranged used Adobe Photoshop CS3 software.

Total RNA Extraction and Small RNA Detection

Total RNA was extracted from the plant tissues using TRIzol reagent (Invitrogen) according to the manufacturer's protocol. For small RNA northern blotting, 10 μg of total RNA was separated on a 15% polyacrylamide/1× Tris-borate/EDTA/8 M urea gel and transferred to a Hybond-N$^+$ membrane. The miR396-AS DNA probe (5′-CAGTTCAAGAAAGCTGTGGAA-3′) and the amiRGFP4-AS DNA probe (5′-TACTCCAATTGGCGATGGCCC-3′) were end labeled with [γ-^{32}P]ATP using T4 polynucleotide kinase (New England Biolabs). Free radioisotopes were filtered out using a mini Quick Spin Oligo Column (Roche). The membrane was hybridized with ULTRAhyb-Oligo hybridization buffer (Ambion) at 42°C for 16 h, and the signal was detected using X-film (GE Healthcare) at −80°C for 16 h.

Real-Time RT-PCR, Semi-RT-PCR, and Northern Blot

For real-time RT-PCR, cDNA was first reverse transcribed from total RNA using oligo(dT)$_{20}$ and the SuperScript III First Strand Synthesis System (Invitrogen). Real-time PCR was performed using a LightCycler 480 instrument (Roche) and three sets of primers for *AtSVP*, *AtGRF1*, and *AtUBQ* expression detection. The primers used for real-time RT-PCR are listed in Supplemental Table S2. For semi-RT-PCR detection, the primers F-CrSVP1_A and R-CrSVP1_C were used to detect *CrSVP1*. The primers F-CrSVP2_A and R-CrSVP2_C were used to detect *CrSVP2*. The primers F-AtSVP and R-AtSVP were used to detect *AtSVP*. The primers F-AdSVP2 and R-AdSVP2 were used to detect *AdSVP2*. The primers CrUBQc-F and CrUBQc-R were used to detect *CrUBQ*. The primers NbActin-F1 and NbActin-R1 were used to detect *NbACTIN*. The primers AtUBQ-F1 and AtUBQ-R1 were used to detect *AtUBQ*. The primers used for semi-RT-PCR are listed in Supplemental Table S3.

Statistical Analyses and Deep Sequencing

The *AtSVP*, *AtGRF1*, and *AtUBQ* transcripts were quantified via a relative cycle threshold (Ct) method. All experiments were performed with three independent replicates to compensate for possible loading errors. The relative expression levels were calculated based on the ΔΔCt value, and each sample was normalized according to the expression level of *AtUBQ*. The miR396 expression levels were normalized via U6 internal/loading controls, which were quantified using ImageQuant 5.2 (GE Healthcare). The ΔΔCt values were used to explain the fold changes in the expression levels.

The small RNA profiles of the *PHYL1* plant, *SAP54* plant, and HF and S4 flowers were analyzed using Illumina HiSeq 2000. The degradome profiles of the Col-0 plant, *CrMIR396* plant, *xrn4-5* mutant, *SAP54* plant, and HF of *C. roseus* plant were also analyzed using Illumina HiSeq 2000. The miRNA and degradome profiles were analyzed using CLC Genomics Workbench 5.5.2 (CLC Bio) and the ContigViews analysis platform (www.contigviews.bioagri.ntu.edu. tw). The read normalization for the miRNA and degradome assays was calculated by the ratio of total reads across various samples to Col-0 plants. The raw small RNA reads reported here have been submitted to the National Center for Biotechnology Information Short Read Archive under accession numbers SRR1818286 (normal flower of Col-0 plant), SRR1818303 (leafy flower of *PHYL1* plant), and SRR1818289 (leafy flower of *SAP54* plant). The raw degradome reads reported are available in the Short Read Archive under accession numbers SRR1821048 (flower of Col-0 plant), SRR1821008 (flower of *CrMIR396* plant), SRR1821172 (flower of *xrn4-5* mutant), SRR1821156 (leafy flower of *SAP54* plant), and SRR1821217 (HF of *C. roseus* plant).

In Situ Hybridization

A digoxigenin (DIG)-labeled *SVP* RNA probe (1,117–1,416 bp) was produced using an in vitro transcription kit (Roche) following the manufacturer's protocol. The embedded Col-0 and *PHYL1* inflorescence tissues were sectioned to 8-μm thickness and hybridized with DIG-labeled RNA probes. The hybridization signal was detected using an anti-DIG antibody conjugated to alkaline phosphatase (Roche) with nitroblue tetrazolium/5-bromo-4-chloro-3-indolyl phosphate as the substrate. The results were examined with a bright-field microscope as purple dotted signals. The protocol followed that of a previous study (Wang et al., 2008).

Supplemental Data

The following supplemental materials are available.

Supplemental Figure S1. Alignment and comparison of the parallel positions of the miR396 target sites from MADS box-containing Arabidopsis genes.

Supplemental Figure S2. In vivo analysis of the miR396-mediated *CrSVP1*, *CrSVP2*, and *AtGRF1* cleavage efficiency by transient expression.

Supplemental Figure S3. In vivo analysis of the miR396-mediated *CrSVP1* expression efficiency by transient expression.

Supplemental Figure S4. Detection of different *SVP* genes in various transgenic plants.

Supplemental Figure S5. Amino acid sequence alignment of AtSVP, CrSVP1, CrSVP2, and AdSVP2.

Supplemental Figure S6. Degradome analysis of Arabidopsis.

Supplemental Figure S7. Degradome data regarding the mismatches in the 5′ portion of the miR396 pairwise region.

Supplemental Table S1. Primers used in this study.

Supplemental Table S2. Primers for real-time RT-PCR.

Supplemental Table S3. Primers for semi-RT-PCR.

LITERATURE CITED

Bao M, Bian H, Zha Y, Li F, Sun Y, Bai B, Chen Z, Wang J, Zhu M, Han N (2014) miR396a-mediated basic helix-loop-helix transcription factor bHLH74 repression acts as a regulator for root growth in Arabidopsis seedlings. Plant Cell Physiol **55:** 1343–1353

Bazzini AA, Lee MT, Giraldez AJ (2012) Ribosome profiling shows that miR-430 reduces translation before causing mRNA decay in zebrafish. Science **336:** 233–237

Bowman JL, Alvarez J, Weigel D, Meyerowitz EM, Smyth DR (1993) Control of flower development in Arabidopsis thaliana by APETALA1 and interacting genes. Development **119:** 721–743

Chang TC (2012) Identification of conserved microRNAs and their targets in PnWB phytoplasma induced leafy flower of Catharanthus roseus. PhD thesis. National Taiwan University, Taipei, Taiwan

Chorostecki U, Crosa VA, Lodeyro AF, Bologna NG, Martin AP, Carrillo N, Schommer C, Palatnik JF (2012) Identification of new microRNA-regulated genes by conserved targeting in plant species. Nucleic Acids Res **40:** 8893–8904

Chung WC, Chen LL, Lo WS, Lin CP, Kuo CH (2013) Comparative analysis of the peanut witches'-broom phytoplasma genome reveals horizontal transfer of potential mobile units and effectors. PLoS ONE **8:** e62770

Debernardi JM, Rodriguez RE, Mecchia MA, Palatnik JF (2012) Functional specialization of the plant miR396 regulatory network through distinct microRNA-target interactions. PLoS Genet **8:** e1002419

Ditta G, Pinyopich A, Robles P, Pelaz S, Yanofsky MF (2004) The SEP4 gene of Arabidopsis thaliana functions in floral organ and meristem identity. Curr Biol 14: 1935–1940

Djuranovic S, Nahvi A, Green R (2012) miRNA-mediated gene silencing by translational repression followed by mRNA deadenylation and decay. Science 336: 237–240

Gregis V, Sessa A, Colombo L, Kater MM (2006) *AGL24, SHORT VEGETATIVE PHASE*, and *APETALA1* redundantly control *AGAMOUS* during early stages of flower development in *Arabidopsis*. Plant Cell 18: 1373–1382

Gregis V, Sessa A, Dorca-Fornell C, Kater MM (2009) The Arabidopsis floral meristem identity genes AP1, AGL24 and SVP directly repress class B and C floral homeotic genes. Plant J 60: 626–637

Guo L, Lu Z (2010) The fate of miRNA* strand through evolutionary analysis: implication for degradation as merely carrier strand or potential regulatory molecule? PLoS ONE 5: e11387

Hartmann U, Höhmann S, Nettesheim K, Wisman E, Saedler H, Huijser P (2000) Molecular cloning of SVP: a negative regulator of the floral transition in Arabidopsis. Plant J 21: 351–360

Himeno M, Neriya Y, Minato N, Miura C, Sugawara K, Ishii Y, Yamaji Y, Kakizawa S, Oshima K, Namba S (2011) Unique morphological changes in plant pathogenic phytoplasma-infected petunia flowers are related to transcriptional regulation of floral homeotic genes in an organ-specific manner. Plant J 67: 971–979

Irish VF (2010) The flowering of Arabidopsis flower development. Plant J 61: 1014–1028

Jang S, Torti S, Coupland G (2009) Genetic and spatial interactions between FT, TSF and SVP during the early stages of floral induction in Arabidopsis. Plant J 60: 614–625

Jones-Rhoades MW, Bartel DP (2004) Computational identification of plant microRNAs and their targets, including a stress-induced miRNA. Mol Cell 14: 787–799

Kidner CA, Martienssen RA (2005) The developmental role of microRNA in plants. Curr Opin Plant Biol 8: 38–44

Lee IM, Davis RE, Gundersen-Rindal DE (2000) Phytoplasma: phytopathogenic mollicutes. Annu Rev Microbiol 54: 221–255

Lee JH, Park SH, Lee JS, Ahn JH (2007a) A conserved role of SHORT VEGETATIVE PHASE (SVP) in controlling flowering time of Brassica plants. Biochim Biophys Acta 1769: 455–461

Lee JH, Yoo SJ, Park SH, Hwang I, Lee JS, Ahn JH (2007b) Role of SVP in the control of flowering time by ambient temperature in Arabidopsis. Genes Dev 21: 397–402

Li D, Liu C, Shen L, Wu Y, Chen H, Robertson M, Helliwell CA, Ito T, Meyerowitz E, Yu H (2008) A repressor complex governs the integration of flowering signals in Arabidopsis. Dev Cell 15: 110–120

Li S, Liu L, Zhuang X, Yu Y, Liu X, Cui X, Ji L, Pan Z, Cao X, Mo B, et al (2013) MicroRNAs inhibit the translation of target mRNAs on the endoplasmic reticulum in Arabidopsis. Cell 153: 562–574

Liang G, He H, Li Y, Wang F, Yu D (2014) Molecular mechanism of microRNA396 mediating pistil development in Arabidopsis. Plant Physiol 164: 249–258

Lin SS, Wu HW, Elena SF, Chen KC, Niu QW, Yeh SD, Chen CC, Chua NH (2009) Molecular evolution of a viral non-coding sequence under the selective pressure of amiRNA-mediated silencing. PLoS Pathog 5: e1000312

Lin YY, Fang MM, Lin PC, Chiu MT, Liu LY, Lin CP, Lin SS (2013) Improving initial infectivity of the Turnip mosaic virus (TuMV) infectious clone by an mini binary vector via agro-infiltration. Bot Stud 54: 22

Liu LY, Tseng HI, Lin CP, Lin YY, Huang YH, Huang CK, Chang TH, Lin SS (2014) High-throughput transcriptome analysis of the leafy flower transition of Catharanthus roseus induced by peanut witches'-broom phytoplasma infection. Plant Cell Physiol 55: 942–957

MacLean AM, Orlovskis Z, Kowitwanich K, Zdziarska AM, Angenent GC, Immink RG, Hogenhout SA (2014) Phytoplasma effector SAP54 hijacks plant reproduction by degrading MADS-box proteins and promotes insect colonization in a RAD23-dependent manner. PLoS Biol 12: e1001835

MacLean AM, Sugio A, Makarova OV, Findlay KC, Grieve VM, Tóth R, Nicolaisen M, Hogenhout SA (2011) Phytoplasma effector SAP54 induces indeterminate leaf-like flower development in Arabidopsis plants. Plant Physiol 157: 831–841

Maejima K, Iwai R, Himeno M, Komatsu K, Kitazawa Y, Fujita N, Ishikawa K, Fukuoka M, Minato N, Yamaji Y, et al (2014) Recognition of floral homeotic MADS domain transcription factors by a phytoplasmal effector, phyllogen, induces phyllody. Plant J 78: 541–554

Mallory AC, Reinhart BJ, Jones-Rhoades MW, Tang G, Zamore PD, Barton MK, Bartel DP (2004) MicroRNA control of PHABULOSA in leaf development: importance of pairing to the microRNA 5′ region. EMBO J 23: 3356–3364

Schwab R, Palatnik JF, Riester M, Schommer C, Schmid M, Weigel D (2005) Specific effects of microRNAs on the plant transcriptome. Dev Cell 8: 517–527

Stefani G, Slack FJ (2008) Small non-coding RNAs in animal development. Nat Rev Mol Cell Biol 9: 219–230

Sugio A, MacLean AM, Kingdom HN, Grieve VM, Manimekalai R, Hogenhout SA (2011) Diverse targets of phytoplasma effectors: from plant development to defense against insects. Annu Rev Phytopathol 49: 175–195

Sunkar R, Kapoor A, Zhu JK (2006) Posttranscriptional induction of two Cu/Zn superoxide dismutase genes in *Arabidopsis* is mediated by downregulation of miR398 and important for oxidative stress tolerance. Plant Cell 18: 2051–2065

Trevaskis B, Tadege M, Hemming MN, Peacock WJ, Dennis ES, Sheldon C (2007) *Short Vegetative Phase*-Like MADS-box genes inhibit floral meristem identity in barley. Plant Physiol 143: 225–235

Voinnet O (2009) Origin, biogenesis, and activity of plant microRNAs. Cell 136: 669–687

Wang CN, Chen YJ, Chang YC, Wu CH (2008) A step-by-step optimization guide for applying tissue specific RNA in-situ hybridization to non-model plant species. Taiwania 53: 383–393

Wang XJ, Reyes JL, Chua NH, Gaasterland T (2004) Prediction and identification of Arabidopsis thaliana microRNAs and their mRNA targets. Genome Biol 5: R65

Wu RM, Walton EF, Richardson AC, Wood M, Hellens RP, Varkonyi-Gasic E (2012) Conservation and divergence of four kiwifruit SVP-like MADS-box genes suggest distinct roles in kiwifruit bud dormancy and flowering. J Exp Bot 63: 797–807

Yang IL (1985) Host responses of peanut witches' broom disease. J Agric Res China 34: 464–468

Zhang X, Garreton V, Chua NH (2005) The AIP2 E3 ligase acts as a novel negative regulator of ABA signaling by promoting ABI3 degradation. Genes Dev 19: 1532–1543

Zhang X, Henriques R, Lin SS, Niu QW, Chua NH (2006) Agrobacterium-mediated transformation of Arabidopsis thaliana using the floral dip method. Nat Protoc 1: 641–646